Paper No.
13425

NACE INTERNATIONAL CORROSION Conference & Expo 2019

Investigation of FeS Precipitation Kinetics by EQCM

Zheng Ma, Bruce Brown, Srdjan Nesic, and Marc Singer
Institute for Corrosion and Multiphase Technology, Ohio University
342 West State Street
Athens, OH, 45701
USA

ABSTRACT

The precipitation kinetics of FeS were studied at varied system temperatures using an Electrochemical Quartz Crystal Microbalance (EQCM). Two different substrates were used for FeS precipitation studies: a cathodically polarized iron-coated quartz crystal, and a freely corroding iron-coated quartz crystal. Precipitation rates were repeatable and consistent when compared at the same temperature. Overall observations show that the precipitation rates of FeS were not very sensitive to the change of temperature. Analysis of the experimental data has also shown that the FeS saturation level on the substrate surface ($S_{FeS,surface}$) should be taken into consideration when the bulk saturation level of FeS ($S_{FeS,bulk}$) was relatively low, as the surface pH could be up to three units higher than the solution pH due to the cathodic polarization. The theoretical kinetic constant and the activation energy for FeS (valid only if $S_{FeS,bulk} > 1$) were determined from the obtained EQCM results based on three possible FeS formation pathways.

Keywords: EQCM, iron carbonate, iron sulfide, precipitation kinetics

INTRODUCTION

Corrosion of carbon steel pipelines in oil and gas applications is often divided into two main categories: sweet corrosion that is mainly caused by aqueous carbon dioxide (CO_2), and sour corrosion which is due to aqueous hydrogen sulfide (H_2S). The formation of corrosion product layers plays a key role in governing the corrosion processes by serving as diffusion barrier, and by affecting the rates of electrochemical reactions occurring on the underlying metal. However, these corrosion product layers are not always protective, especially when the metal underneath is suffering from rapid corrosion. It has been suggested that the protectiveness of a corrosion product layer is dependent on the competition between the precipitation rate and corrosion rate of the underlying substrate metal[1]. Therefore, a better understanding of the factors governing the rate of corrosion product layer formation would help develop more efficient corrosion mitigation methods.

Increased attention has been brought to H_2S corrosion in recent years, not only because newly discovered sources of oil and gas usually contain significant concentrations of H_2S, but also because the understanding of H_2S related corrosion processes is very limited. Despite the fact that large numbers of papers have been published on this topic[2-11], little research of the formation kinetics of sour corrosion products, typically iron sulfides (FeS), has been conducted.

According to the most recent developments, the mechanism of FeS formation on a steel substrate follows a two steps process[12]: the formation of a chemisorbed FeS film followed by the precipitation of a FeS layer. The chemisorption step generates a very thin film (nanometer range thickness) while the precipitated FeS layer can reach several microns in thickness. When investigating the formation kinetics using mass change techniques, the effect of the precipitation process naturally overwhelms the measurements. Consequently, the generated kinetics equations are only representing the process of FeS precipitation.

FeS forms easily due to a relative low solubility and fast precipitation kinetics as compared to that of iron carbonate ($FeCO_3$), the main corrosion product found in sweet corrosion environment. Among different types of iron sulfides[13-15], even the most soluble phase of FeS, mackinawite[16, 17], has been observed to precipitate within the order of seconds[3, 18, 19]. According to Harmandas *et al.*[20], the apparent precipitation rate exhibited a 2nd order dependence on the relative solution supersaturation of iron sulfide at 25°C. But with an increase in temperature to 80°C, the measured reaction order of precipitation decreased to 1. In all conditions, the authors identified the corrosion product as mackinawite. An estimated activation energy of 40 kJ/mol was also suggested from the Harmandas *et al.*[20] study. However, the results were obtained from a homogeneous precipitation process (*i.e.*, precipitation from bulk solution), which could be very different from a heterogeneous precipitation process (*i.e.*, precipitation on the substrate surface), which occurs more readily in an oil and gas pipeline.

Models have been proposed to predict the kinetics of FeS precipitation. Based on the observation from Harmandas *et al*., Lee[4] proposed an expression for mackinawite precipitation rate (PR_{FeS}, in the unit of *mol·m*$^{-2}$*·s*$^{-1}$) calculation that includes both the effect from temperature (in kelvin) and solution saturation of mackinawite (S_{FeS}):

$$PR_{FeS} = 11.5 \times e^{-\frac{9520.648}{T_K}} (S_{FeS}^{0.5} - 1)^2 \quad (1)$$

where the supersaturation for mackinawite can be calculated by:

$$S_{FeS} = \frac{[Fe^{2+}][S^{2-}]}{K_{sp,FeS(S^{2-})}} \quad (2)$$

with the $K_{sp,FeS(S^{2-})}$ in $(mol/L)^2$ being the solubility of mackinawite:

$$K_{sp,FeS(S^{2-})} = [Fe^{2+}]_{eq}[S^{2-}]_{eq} \quad (3)$$

Later on, Zheng proposed a new expression based on an analogy with the S&N $FeCO_3$ model[21] to calculate the mackinawite layer precipitation rate[12]:

$$PR_{FeS} = k_{r,Fes} \times e^{-\frac{40000}{RT}} K_{sp,S^{2-}} (S_{FeS} - 1) \quad (4)$$

In this expression, the solubility limit of mackinawite, $K_{sp,S^{2-}}$, is determined from Benning's Equation[8], and the kinetic constant $k_{r,Fes}$=7.02×10^{14} $m^4 \cdot mol^{-1} \cdot s^{-1}$ was calibrated with corrosion rate measurements[5]. However, no experimental precipitation data has been published to support this expression, which makes its accuracy questionable without comprehensive validation. Therefore, a comprehensive understanding of the FeS layer precipitation kinetics is necessary. The FeS considered in this study is limited to mackinawite, as the mackinawite is the most common and first product formed in the sour environment.

The equations listed above, especially Equation (1) and Equation (4), were proposed based on experimental results obtained in H_2S only environment. However, they are commonly applied to sour environments which also include the presence of CO_2 [4, 5]. The possible competitive effects between FeS and $FeCO_3$ precipitation have not been fully understood yet. However, since FeS formation has much faster precipitation kinetics than that of $FeCO_3$, it is reasonable to assume that these models are still valid in the H_2S dominated environment even in the present of CO_2.

In the current work, a very accurate device, electrochemical quartz crystal microbalance (EQCM), was used to monitor the *in-situ* mass change. Theoretically, a nano-scale mass change on the quartz crystal surface leads to a detectable change in its oscillation frequency. According to Sauerbrey's Equation[22], there is a linear relationship between the mass change on the quartz crystal surface and its oscillation frequency change:

$$\Delta f = -C_f \cdot \Delta m \tag{5}$$

where the Δf is frequency change (*Hz*), C_f is the sensitivity factor for the quartz crystal ($Hz \cdot \mu g^{-1} \cdot cm^2$), and Δm is the change in mass per unit area ($\mu g \cdot cm^{-2}$).

Besides the ability of monitoring the *in-situ* mass change in high resolution, the EQCM also allows simultaneous electrochemical measurements[23, 24]. This makes the EQCM a suitable tool for the current research.

EXPERIMENTAL

Methodology

The methodology developed for using the EQCM to study the precipitation kinetics of FeS is presented in this section. To differentiate the various effects on corrosion precipitation as detected by the EQCM mass change, two sets of experiments were designed using two different substrates. In addition, the experiments were performed at different temperatures so that the effects on the precipitation kinetics of FeS could be defined over a range of conditions.

Experimental set #1: FeS precipitation on a cathodically protected iron (Fe)-coated quartz crystal surface where a negative potential *vs.* its OCP was applied and held during the experiment. This substrate is close in nature to the carbon steel surface. The substrate corrosion was minimized by the polarization and the precipitation of FeS was the dominant process affecting the EQCM measurements.

Experimental set#2: FeS precipitation on an actively corroding iron (Fe)-coated quartz crystal surface. This is a more realistic situation, where both the FeS precipitation and spontaneous iron corrosion were occurring simultaneously at the substrate surface.

Apparatus

The EQCM device by Stanford Research System† (QCM200) was used. The Fe-coated quartz crystals with a 1.37 cm^2 effective area is shown in Figure 1. Before the experiment, the quartz crystal was installed into the crystal holder and immersed into a 2-liter glass cell (Figure 2) to serve as the working electrode. A surface to volume (S/V) ratio of 1460 mL/cm^2 was reached, which is sufficiently high to ensure that the precipitation/dissolution of the FeS will not affect the properties of solution[25]. A saturated Ag/AgCl electrode was used as the reference electrode and the counter electrode was a platinum wire mesh as shown in the figure. The solution pH was monitored through a pH probe immersed in the electrolyte. A desired H_2S concentration was maintained by a sparge tube through the entire duration of the experiment. The temperature of the solution was controlled by an immersed thermocouple connected to a heating plate.

Figure 1: Iron-coated quartz crystal

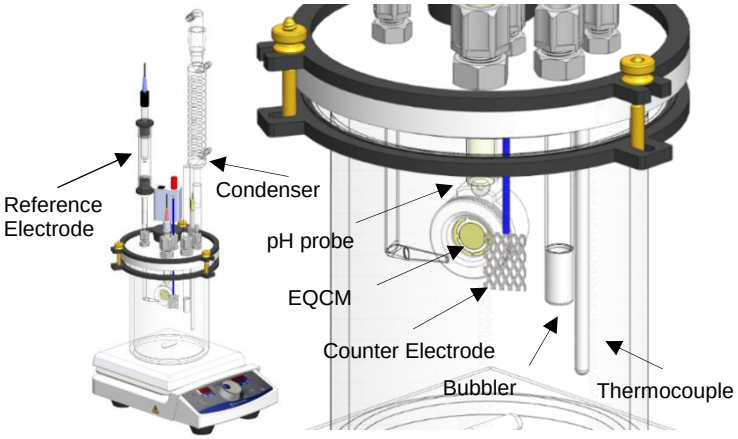

Figure 2: Experimental set-up with EQCM (Image courtesy of Cody Shafer, ICMT).

Procedure

The experimental matrix for the three sets of FeS precipitation experiments is shown in Table 1. All the experiments were conducted in a 2-liter glass cell filled with 1wt.% NaCl solution. The solution was de-aerated by sparging with N_2 for at least two hours to ensure the oxygen concentration in the solution was less than 10 ppb, followed by sparging with a mixture of H_2S/N_2 to saturate the bulk solution at a desired

† Trade Name

H_2S partial pressure. After the solution temperature was set to the desired value, the solution pH was adjusted to 6.6 by adding a deoxygenated NaOH solution. The value of the solution pH is typical of environments encountered in oil and gas production (5 to 7) but was also selected to ensure that relatively high FeS saturation values could be achieved easily. The quartz crystal was cleaned with a N_2 gas stream before each test to remove any dust from the surface. The working electrode potential was adjusted using a potentiostat (Gamry Reference 600™†). A deaerated ferrous chloride ($FeCl_2 \cdot 4H_2O$) solution was added to adjust the Fe^{2+} concentration and S_{FeS}. The bulk solution pH was measured *in situ* as solution samples were drawn periodically from the glass cell to record the change Fe^{2+} concentration. When using the actively corroding iron coated quartz crystal, linear polarization resistance (LPR) with scan rate of 0.125mV/s was employed to measure the corrosion rate using a B value of 23 mV/decade. The choice of the correct "B" value can be difficult especially if conditions are changing during the experiment, as it is the case in this study. A "B" value of 23 mV/decade has been validated in conditions similar to the ones tested in this work[12]. The LPR results should therefore be viewed qualitatively.

Table 1
Experimental Matrix for FeS Precipitation on Different Substrates.

Description	Parameters	
Solution	1wt.% NaCl	
Total pressure/bar	1	
H_2S partial pressure/ppm	100	
Initial solution pH	6.6±0.05	
Stir bar stirring speed/rpm	250	
Materials	Polished Fe-coated quartz crystal	
Temperature/°C	30-80	
Initial [Fe^{2+}]/ppm	15~30	
Polarization/V	-0.05~-0.1 *vs.* OCP	None (0 *vs*. OCP)
Test Duration/day	1-3	

Procedure for FeS Precipitation Rate Calculation

The methodology of calculating the precipitation rate of FeS from EQCM measurements is illustrated in Figure 3, by taking FeS precipitation at 30°C on an actively corroding Fe-coated quartz crystal surface as an example. During the test, the pH value and [Fe^{2+}] in the bulk solution were measured multiple times to get the bulk saturation value of FeS ($S_{FeS,bulk}$) according to Equation (2). Given that the accuracy of measuring the Fe^{2+} concentration was ±1% of the measurement range, and the accuracy of the pH

† Trade Name

measurement was approximately 0.05 pH unit, the error in the saturation value was estimated at 12% as indicated in all the graphs using error bars. The error in measuring the mass change using the EQCM was not accounted for as the error was too small to be adequately shown on the plots.

As shown in Figure 3, the mass change monitored by EQCM increased due to the FeS precipitated on the surface of the quartz crystal. Each time when the saturation of FeS was measured, the instantaneous slope (mass change per unit area *vs*. time) at each specific time was calculated and used to determine the precipitation rate and the corresponding saturation value. The measured precipitation rates having the unit of $\mu g \cdot cm^{-2} \cdot s^{-1}$ were converted to $mol \cdot m^{-2} \cdot s^{-1}$ for easier comparison with literature data[21, 12]. Even though the precipitation is a two-step process that includes both crystal nucleation and crystal growth[26] , the current work aims at finding the precipitation rate during the crystal growth period only, as the nucleation step is usually short and surface preparation dependent[27]. In addition, the crystal growth step is a process that is more relevant to the understanding of the corrosion product layer formation[28] .

When using an actively corroding Fe-coated quartz crystal, the calculated precipitation rate would appear to be lower than its true value if the EQCM captured mass gain were to be used directly without compensation for mass loss due to corrosion. The total mass change captured by the EQCM is equal to the precipitation mass gain minus the corrosion mass loss. A mass compensation protocol was put in place to address this issue whenever an actively corroding Fe-coated quartz crystal was used: the mass loss was calculated from the LPR measured corrosion rate data and then added to the mass gain recorded by EQCM. The obtained new value was used for precipitation rate calculation.

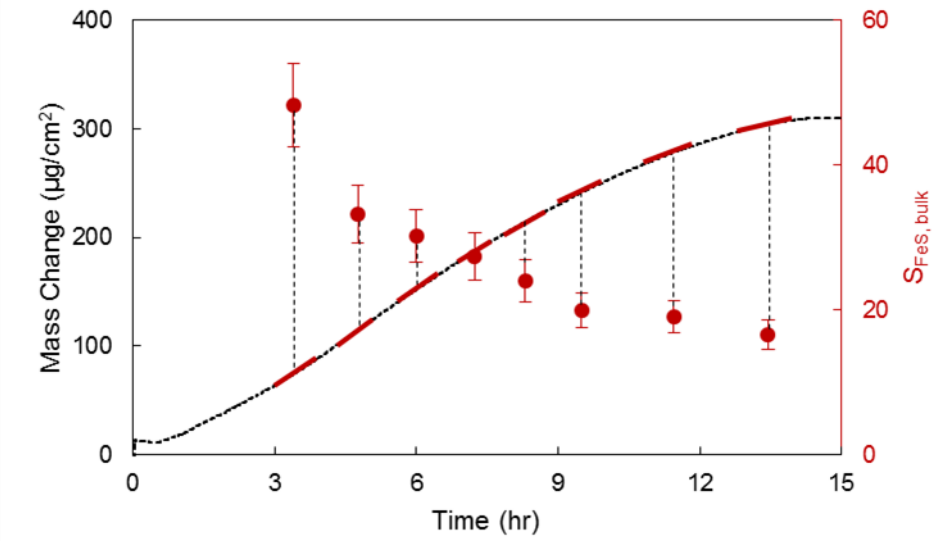

Figure 3: Illustration of FeS precipitation rate calculation methodology using EQCM on a polarized Fe-coated quartz crystal, initial solution pH 6.6, 30°C.

EXPERIMENTAL RESULTS AND DISCUSSION

EQCM Measured Precipitation Kinetics of FeS

By making the analogy to the $FeCO_3$ precipitation kinetics, the precipitation kinetics of FeS should be related to $S_{FeS, bulk}$ and system temperature. In this section, the results of FeS precipitation kinetics on both substrates are discussed at different temperatures.

Comparisons of PR_{FeS} *vs.* $S_{FeS,\,bulk}$ on both substrates are presented in Figure 4 for all tested temperatures, and several similarities can be extracted from the results from 40°C to 80°C. Based on the data from the actively corroding Fe-coated crystal, the measured PR_{FeS} exhibits an approximately linear dependence on the $S_{FeS,\,bulk}$, as the exponent with respect to $S_{FeS,\,bulk}$ of around 1 (0.75-1.31) was obtained through the best fit lines (shown as green dotted lines for each temperature). When using the polarized Fe-coated crystal, a mass gain was observed during the entire experiment duration for all the temperatures (blue dashed lines). This suggests that FeS was able to precipitate on the polarized Fe-coated crystal even when the $S_{FeS,\,bulk}$<1. Figure 4 shows the results obtained between $S_{FeS,\,bulk}$=1 and $S_{FeS,\,bulk}$=100; dashed lines are applied for the polarized results which represent the data beyond this domain. By using cathodic polarization (protection), the substrate corrosion was largely reduced and it is understood that the surface pH was also increased, which increased FeS precipitation as compared to a substrate without the polarization at same bulk conditions. This also explains why the PR_{FeS} on a polarized substrate surface was less dependent on $S_{FeS,\,bulk}$ as compared with the actively corroding surface. When applying cathodic polarization, $S_{FeS,\,bulk} < S_{FeS,\,surface}$ where the precipitation process was taking place. When comparing the precipitation rate of FeS between different substrates, most of the measured precipitation rates on the actively corroding Fe-coated crystal were considerably lower than the ones obtained on the polarized Fe-coated quartz crystal. This was also due to the fact that the precipitation rate of FeS on an actively corroding Fe-coated crystal was affected by the spontaneous iron substrate dissolution, which made it harder to nucleate. This means that the measured mass change was affected by both the mass loss due to corrosion and by the mass gain due to precipitation. The derived FeS formation rates (unless they are compensated, as shown previously in the text) will consequently underpredict the true kinetics of precipitation. In addition, the discrepancies of the FeS precipitation kinetics on different substrate surfaces became larger at lower $S_{FeS,\,bulk}$ as the precipitation process was affected more by the substrate surface speciation. Similar phenomenon has been observed during the study of $FeCO_3$ precipitation kinetics[21, 29].

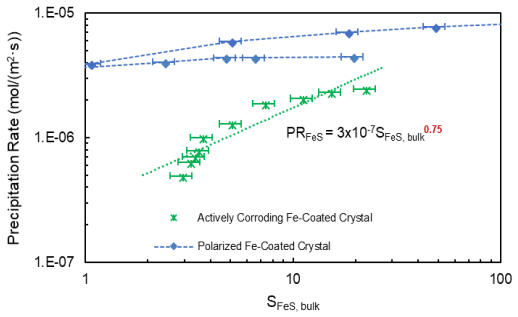

80°C

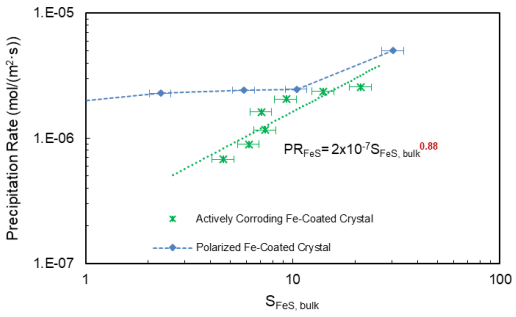

70°C

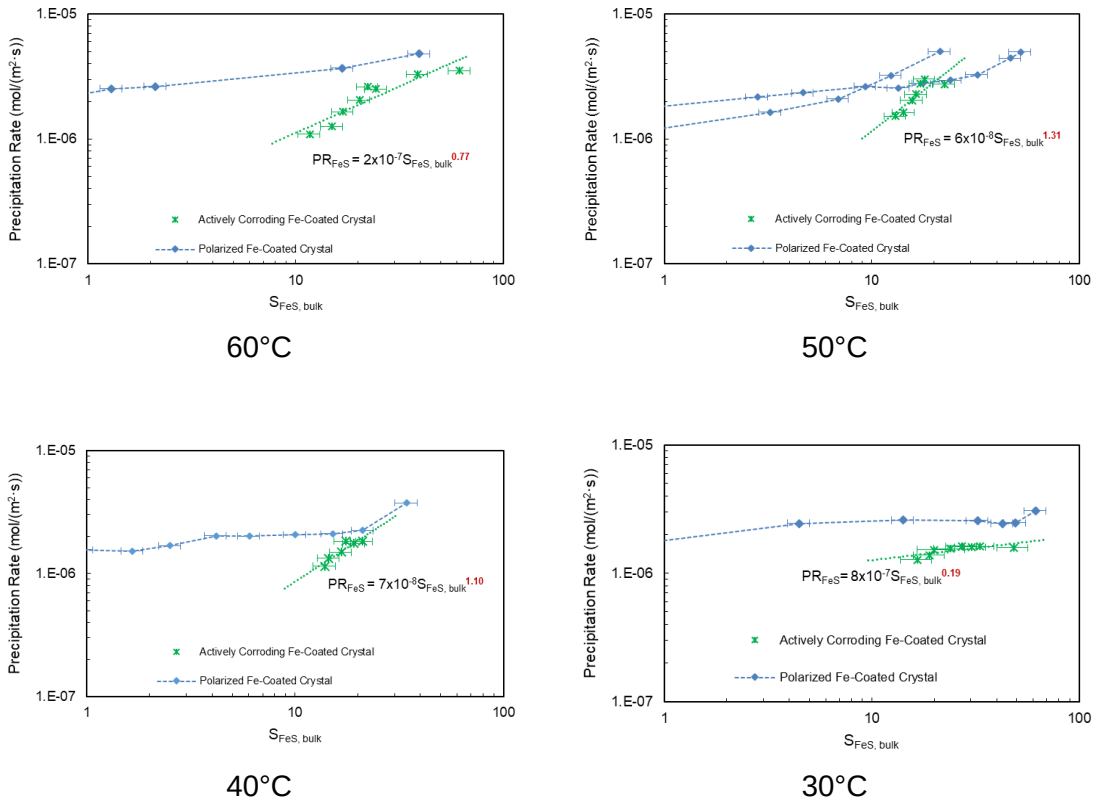

Figure 4: Precipitation rates comparison between two substrate surfaces at different temperatures.

When the temperature was decreased to 30°C, the precipitation rate seemed independent of the $S_{FeS,\ bulk}$ (*ie.*, the exponent with respect to $S_{FeS,\ bulk}$≈0). Figure 5 presents both the compensated PR_{FeS} (as presented in the "Procedure for FeS Precipitation Rate Calculation" section) and the PR_{FeS} before compensation *vs.* $S_{FeS,bulk}$ on an actively corroding Fe-coated crystal at 30°C. It can be seen that the PR_{FeS} was up to 5 times larger after applying compensation for the total mass change rate and was affected more by the compensation at lower $S_{FeS,bulk}$. This suggests that the total precipitation mass gain rate was mainly influenced by the corrosion mass loss rate, especially at lower $S_{FeS,bulk}$. By checking the corrosion rate as shown in Figure 6, it can be seen that the corrosion rate during the measurement was almost constant, and this created an almost constant PR_{FeS}. The stable corrosion rate also implied that the precipitated FeS layer in this case did not provide strong protection to the substrate surface.

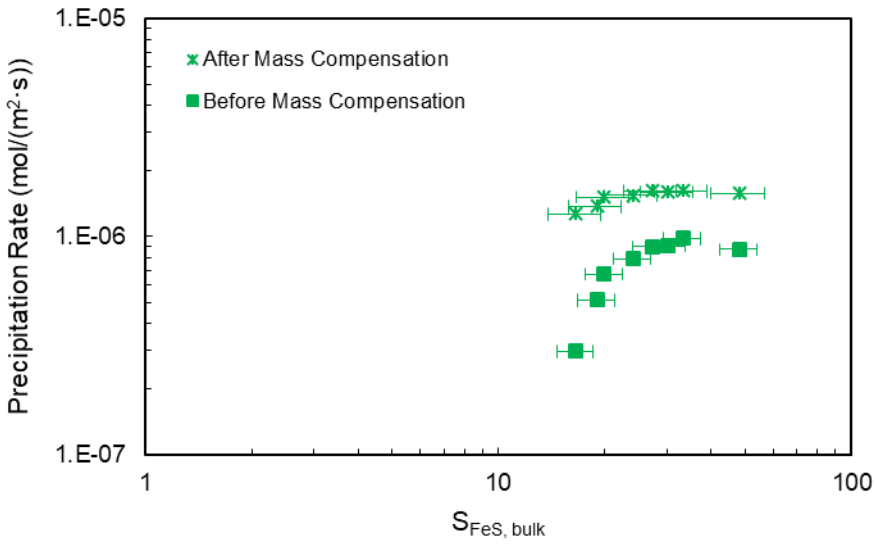

Figure 5: Precipitation kinetics of FeS on actively corroding Fe-coated crystal, 30°C.

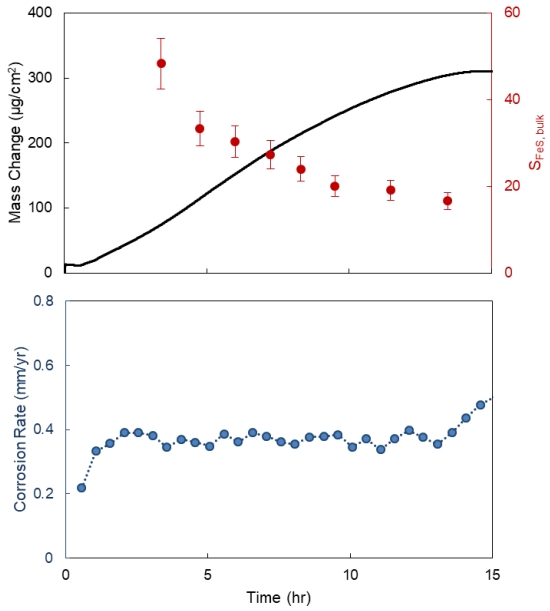

Figure 6: Corrosion rate during the FeS precipitation at 30°C.

Calculation of Surface speciation (Free of Corrosion Product Layer)

As mentioned in the last section, instead of using the bulk solution conditions, the surface speciation had to be taken into consideration, especially when studying the precipitation kinetics of FeS in a lower

$S_{FeS,\ bulk}$ condition, or when FeS precipitated on a polarized substrate surface. This section explains the procedure to calculate the surface speciation under polarization, as well as compares the results between bulk conditions and surface speciation. At this stage, the calculation covers the surface speciation without considering the effect from corrosion product layer formation.

The idea of two-node model proposed by Zheng *et al.*[5], as shown in Figure 7 is used as a starting point for the calculations. It starts with a mass conservation equation at the steel surface:

$$\frac{\partial c_{surface,j}}{\partial t} = \frac{N_{in,j} - N_{out,j}}{\Delta x} + R_j \tag{6}$$

Where $c_{surface,j}$ is the species concentration on the steel surface, $N_{in,j}$ is the mass transfer flux from bulk to surface, $N_{out,j}$ is the flux due to heterogeneous electrochemical reactions, R_j is the production due to homogeneous chemical reactions, and Δx represents the boundary layer thickness between the steel surface and bulk solution. In this model, the species concentration in the bulk solution, $c_{bulk,j}$, was calculated from bulk water chemistry model[12].

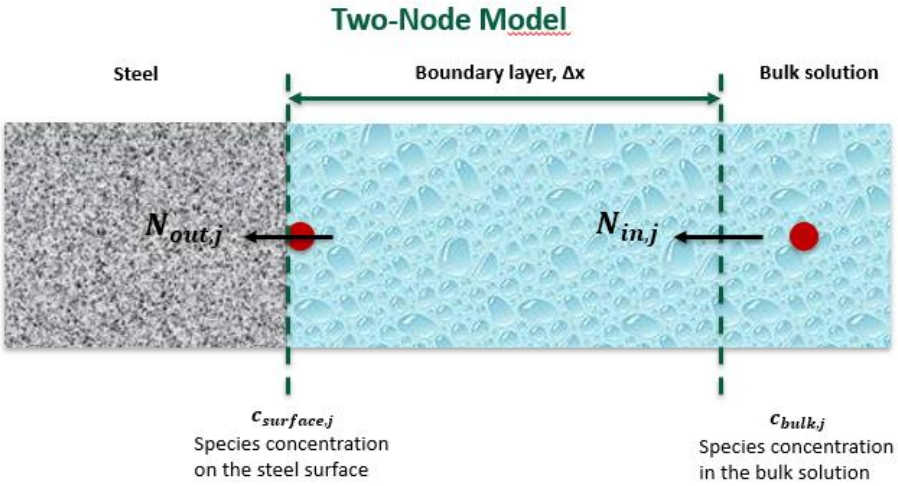

Figure 7: Illustration for the mass transport governing equation and computation domain.

In Zheng's original model[5], the surface concentrations for all related species were presented as a function of corrosion potential and the surface concentration of H^+. Then the species surface concentrations were solved through a simplified mass balance equation of H^+. The corrosion potential, E_{corr}, was solved by the current balance equation (*ie.*, anodic current density=cathodic current density). Finally, all the related species concentrations on the steel surface were checked by satisfying the charge neutrality equation. By using this methodology, the surface condition could be calculated at the corrosion potential.

The basic methodology of the current model is equivalent to Zheng's[5], but instead of solving E_{corr} through the current balance equation, the applied potential, E_{app}, was used as a known parameter during process. Therefore, the surface condition was predicted at a desired potential rather than at E_{corr} only .

The calculated surface pH can now be compared with measured bulk pH during precipitation experiments at 80°C and 30°C. As shown in Figure 8, the calculated surface pH was initially about 2-3 units higher than the bulk pH due to the cathodic polarization, this applies at both temperatures. With increasing time, the measured bulk pH decreased during the precipitation process and so that the final bulk pH was more than 1 unit lower than its initial value. However, the changes for the calculated surface pH were much smaller, as most of the generated H^+ on the steel surface were immediately consumed by the polarization generated electrons-*i.e.*, the cathodic polarization "buffered" the pH change on the substrate surface by accelerating H^+ reduction rate and made the surface speciation very different from the bulk conditions. The surface pH is expected to be higher due to the acceleration of the cathodic reactions under polarization. This explains the relatively weak dependency between the PR_{FeS} and the $S_{FeS,bulk}$ when using cathodically polarized Fe-coated crystal: the bulk conditions cannot adequately reflect the actual conditions where the precipitation was taking place.

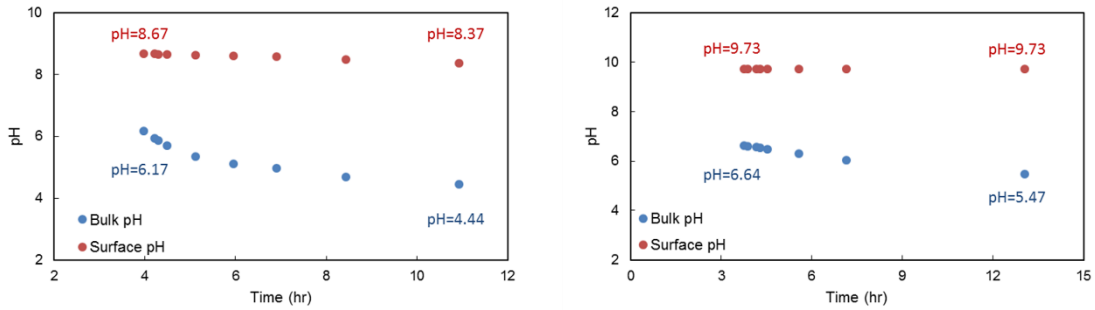

80°C, -815mV 30°C, -830mV

Figure 8: Measured bulk pH *vs.* calculated surface pH during precipitation.

Future studies will require modifications to some assumptions used in this study. In order to obtain a more accurate prediction of the surface speciation, the effect of corrosion product precipitation (sink of Fe^{2+} ions) on the solution chemistry also needs to be taken into consideration. In addition, the mass transfer coefficients for species used in the current calculations were taken from a system with a rotating cylinder electrode. The corresponding coefficients must be measured for the EQCM system to improve the accuracy of the model's prediction.

ACTIVATION ENERGY AND KINETIC CONSTANT IN THE PRECIPITATION RATE EQUATIONS

The modeling of the FeS precipitation kinetics was currently done based on the bulk conditions since the calculation of more accurate surface speciation will require further studies. Consequently, the following derivation is believed to be applicable only in case where the bulk saturation with regard to FeS is larger than 1. In addition, the model was validated over a specific range of conditions: 30°C<T<80°C, 1wt% NaCl, 1 bar total pressure, mackinawite only.

Based on the solubility limit expressions of mackinawite, the formation of mackinawite can be expressed through different reactions as shown in Equation (7) for "H_2S - Equation", Equation (9) for "HS^-- Equation", and Equation (11) for "S^{2-} - Equation", with their corresponding solubility limit expressions defined in Equation (8), Equation(10), and Equation (3), respectively [30].

$$Fe^{2+}_{(aq)} + H_2S_{(aq)} \rightleftharpoons FeS_{(s)} + 2H^+_{(aq)} \quad (7)$$

$$K_{sp,FeS(H_2S)} = \frac{[Fe^{2+}][H_2S]}{[H^+]^2} \quad (8)$$

$$Fe^{2+}_{(aq)} + HS^-_{(aq)} \rightleftharpoons FeS_{(s)} + H^+_{(aq)} \quad (9)$$

$$K_{sp,FeS(HS^-)} = \frac{[Fe^{2+}][HS^-]}{[H^+]} \quad (10)$$

$$Fe^{2+}_{aq} + S^{2-}_{aq} \rightleftarrows FeS_{(s)} \quad (11)$$

$$K_{sp,FeS(S^{2-})} = [Fe^{2+}]_{eq}[S^{2-}]_{eq} \quad (3)$$

The expressions of the mackinawite solubility limit can be converted into each other using dissociation constants as defined through Equation (12) and (13):

$$K_{sp,FeS(HS^-)} = K_{sp,FeS(H_2S)}K_{a,1} \quad (12)$$

$$K_{sp,FeS(S^{2-})} = K_{sp,FeS(H_2S)}K_{a,1}K_{a,2} \quad (13)$$

In which the first dissociation constant of H_2S is defined as:

$$K_{a,1} = \frac{[H^+][HS^-]}{[H_2S]} \quad (14)$$

Its value can be calculated through the expression[31]:

$$K_{a,1} = 10^{782.43945+0.36126T_k-0.00016722T_k^2-20565.7315T_k-142.7417222Log(T_k)} \quad (15)$$

And the second dissociation constant is defined as:

$$K_{a,2} = \frac{[H^+][S^{2-}]}{[HS^-]} \quad (16)$$

With the value can be calculated from[32]:

$$K_{a,2} = 10^{23.93-0.030446T_k+2.4831\times10^{-5}T_k^2} \quad (17)$$

The $K_{sp,FeS(H_2S)}$ used in this work was calculated using the following equation proposed by Benning *et al.*[8]:

$$K_{sp,FeS(H_2S)} = 10^{\frac{2848.779}{T_K}-6.347} \quad (18)$$

Based on different formation reactions of FeS, Equation (19) is proposed to calculate the precipitation rate of FeS formed through the H_2S - Equation, Eq (7):

$$PR_{FeS_{(H_2S)}} = k_{r(H_2S)} e^{\left(-\frac{\Delta G_{(H_2S)}}{RT}\right)} [H^+]^2 K_{sp,FeS(H_2S)} (S_{FeS} - 1) \quad (19)$$

Equation (20) is proposed to calculate the precipitation rate of FeS formed through the HS^-- Equation, Eq (9):

$$PR_{FeS_{(HS^-)}} = k_{r(HS^-)} e^{\left(-\frac{\Delta G_{(HS^-)}}{RT}\right)} [H^+] K_{sp,FeS(HS^-)} (S_{FeS} - 1) \quad (20)$$

And Equation (21) is proposed to calculate the precipitation rate of FeS formed through the S^{2-} - Equation, Eq (11):

$$PR_{FeS_{(S^{2-})}} = k_{r(S^{2-})} e^{\left(-\frac{\Delta G_{(S^{2-})}}{RT}\right)} K_{sp,FeS(S^{2-})} (S_{FeS} - 1) \quad (21)$$

If these three equations are closely compared, one should notice that the $PR_{FeS_{(H_2S)}}$ in Equation (19) is highly dependent on $[H^+]$ change, the $PR_{FeS_{(HS^-)}}$ in Equation (20) is linearly dependent on the change of $[H^+]$, and the $PR_{FeS_{(S^{2-})}}$ in Equation (21) is not dependent on $[H^+]$ change at all. In addition, for all three proposed equations, the PR_{FeS}, $[H^+]$, $K_{sp,FeS}$, and S_{FeS} can be either measured from the experimental results, or can be calculated from a water chemistry model. That leaves only two unknowns for each equation: the kinetic constant, k_r, and the activation energy, ΔG.

To obtain the values for unknowns, a natural logarithm applied on both sides of the precipitation rate equation, and Equation (22) can be derived if from Equation (19), the H_2S based expression, as an example:

$$ln \frac{PR_{FeS}}{K_{sp,FeS(H_2S)}(S_{FeS} - 1)[H^+]^2} = -\frac{\Delta G_{(H_2S)}}{RT} + ln\, k_{r(H_2S)} \quad (22)$$

Therefore, a plot of $ln \frac{PR_{FeS}}{K_{sp,FeS(H_2S)}(S_{FeS}-1)[H^+]^2}$ *vs.* $(\frac{1}{RT})$ should theoretically show a straight line with the slope equals to the activation energy $-\Delta \boldsymbol{G}$ and the y intercept equals to $\ln k_r$. This is shown in Figure 9 for each expression as noted. The best fit line yielded ΔG and k_r, which are summarized and compared in Table 2 including the R-squared value from the fitted lines. According to this analysis, the values of ΔG are very similar (ranging between 33-42 kJ/mol), but the value of k_r varies by about 8 orders of magnitude between the one obtained from from S^{2-} - expression and the HS^- - expression and about 11 orders of magnitude from the H_2S - expression. In addition, the k_r from the S^{2-} - expression logically agrees best with the value used in Equation (4). However, this agreement does not necessarily suggest or verify the kinetics model proposed in Equation (4) or Equation (21), since no experiment has been conducted to study the dependency between PR_{FeS} and $[H^+]$.

Table 2
Comparison of experimental extracted k_r and ΔG in different FeS precipitation reactions.

Reactions	k_r ($m^4mol^{-1}s^{-1}$)	ΔG (kJ/mol)	R^2
$Fe^{2+}_{(aq)} + H_2S_{(aq)} \rightleftharpoons FeS_{(s)} + 2H^+_{(aq)}$	3.7x10^2	33	0.64

$Fe^{2+}_{(aq)} + HS^{-}_{(aq)} \rightleftharpoons FeS_{(s)} + H^{+}_{(aq)}$	2.4x10^{5}	42	0.89
$Fe^{2+}_{aq} + S^{2-}_{aq} \rightleftarrows FeS_{(s)}$	5.8x10^{13}	36	0.79

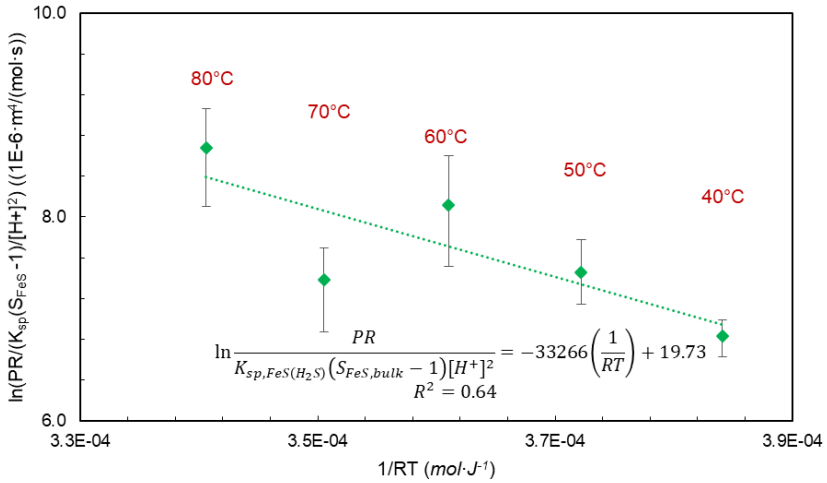

(a). $Fe^{2+}_{(aq)} + H_2S_{(aq)} \rightleftharpoons FeS_{(s)} + 2H^{+}_{(aq)}$

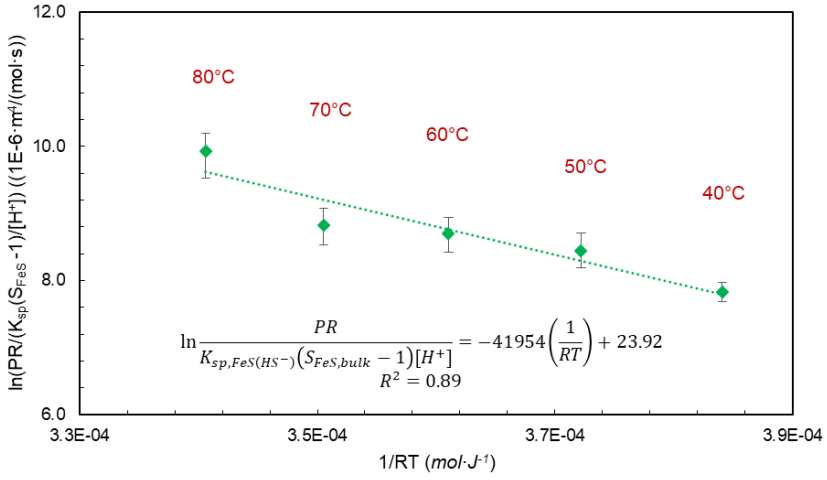

(b). $Fe^{2+}_{(aq)} + HS^{-}_{(aq)} \rightleftharpoons FeS_{(s)} + H^{+}_{(aq)}$

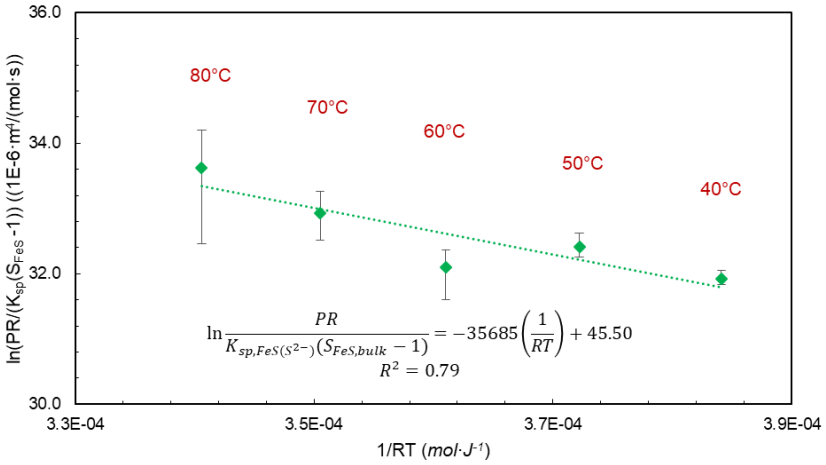

(c). $Fe^{2+}_{aq} + S^{2-}_{aq} \rightleftarrows FeS_{(s)}$

Figure 9: Graphical analysis for activation energy and kinetic constant in different FeS precipitation rate equations.

CONCLUSIONS

- A linear relationship between PR_{FeS} and $S_{FeS,bulk}$ was observed in test conditions from 40°C to 80°C when using an actively corroding iron substrate.
- FeS precipitation rates were detected even if $S_{FeS,bulk} < 1$, suggesting that surface speciation plays a very important role, especially in under-saturated environments.
- A methodology to calculate the water chemistry surface speciation of a metal surface under potentiodynamic polarization was proposed for a corrosion product layer-free condition.
- Kinetics models for FeS precipitation were proposed considering different possible FeS precipitation pathways. These models are only valid in conditions where $S_{FeS,bulk} > 1$.

ACKOWLEDGEMENTS

Anadarko, Baker Hughes, BP, Chevron, CNOOC, ConocoPhillips, DNV GL, ExxonMobil, M-I SWACO (Schlumberger), Multi-Chem (Halliburton), Occidental Oil Company, PTT, Saudi Aramco, SINOPEC (China Petroleum), and TOTAL.

REFERENCES

[1] E. W. J. v. Hunnik, B. F. M. Pots, and E. L. J. A. Hendriksen, "The Formation of Protective $FeCO_3$ Corrosion Product Layers In CO_2 Corrosion," CORROSION/1996, paper no. 6, (Houston, Texas, 1996).

[2] H. Ma, X. Cheng, G. Li, S. Chen, Z. Quan, S. Zhao, *et al.*, "The influence of hydrogen sulfide on corrosion of iron under different conditions," *Corrosion Science*, vol. 42, (2000), pp. 1669-1683.

[3] K.-L. Lee and S. Nešić, "EIS Investigation on the Electrochemistry of CO_2/H_2S Corrosion," CORROSION/2004, paper no. 04728, (New Orleans, Louisiana, 2004).

[4] K.-L. J. Lee, "A Mechanistic Modeling of CO_2 Corrosion of Mild Steel in the Presence of H_2S," Ph.D. Dissertation, Dept. Chem. Eng., Ohio Univ., Athens, OH, 2004.

[5] Y. Zheng, J. Ning, B. Brown, and S. Nešić, "Advancement in predictive modeling of mild steel corrosion in CO_2- and H_2S- containing environments," *Corrosion*, vol. 72, (2016), pp. 679-691.

[6] H. Fang, B. Brown, and S. Nešic, "High Salt Concentration Effects on CO_2 Corrosion and H_2S Corrosion," CORROSION/2010, paper no. 10276, (San Antonio, Texas, 2010).

[7] A. R. Lennie, S. Redfern, P. Champness, C. Stoddart, P. Schofield, and D. Vaughan, "The influence of hydrogen sulfide on corrosion of iron under different conditions," *American Mineralogist*, vol. 82, (1997), pp. 302-309.

[8] L. G. Benning, R. T. Wilkin, and H. L. Barnes, "Reaction pathways in the Fe–S system below 100°C," *Chemical Geology*, vol. 167, (2000), pp. 25-51.

[9] C. Ren, D. Liu, D. Liu, and T. Li, "Corrosion behavior of oil tube steel in simulant solution with hydrogen sulfide and carbon dioxide," *Materials Chemistry and Physics*, vol. 93, (2005), pp. 305-309.

[10] W. Sun and S. Nešić, "A Mechanistic Model of H_2S Corrosion of Mild Steel," CORROSION/2007, paper no. 07655, (Nashiville, Tennessee, 2007).

[11] J. Amri and J. Kvarekvål, "Simulation of Solid-State Growth of Iron Sulfides in Sour Corrosion Conditions," CORROSION/2011, paper no. 11078, (Houston, Texas, 2011).

[12] Y. Zheng, "Electrochemical Mechanism and Model of H_2S Corrosion of Carbon Steel," Ph.D. Dissertation, Dept. Chem. Eng., Ohio Univ., Athens, OH, 2015.

[13] S. Gao, B. Brown, D. Young, and M. Singer, "Formation of iron oxide and iron sulfide at high temperature and their effects on corrosion," *Corrosion Science*, vol. 135, (2018), pp. 167-176.

[14] J. Ning, Y. Zheng, D. Young, B. Brown, and S. Nesic, "A Thermodynamic Study of Hydrogen Sulfide Corrosion of Mild Steel," CORROSION/2013, paper no. 2462, (Orlando, Florida, 2013).

[15] J. Ning, Y. Zheng, B. Brown, D. Young, and S. Nesic, "Construction and Verification of Pourbaix Diagrams for Hydrogen Sulfide Corrosion of Mild Steel," CORROSION/2015, paper no. 5507, (Dallas, Texas, 2015).

[16] Z. Dai, A. T. Kan, W. Shi, N. Zhang, F. Zhang, F. Yan, *et al.*, "Solubility measurements and predictions of gypsum, anhydrite, and calciteover wide ranges of temperature, pressure, and ionic strength with mixed electrolytes," *Rock Mechanics and Rock Engineering*, vol. 50, (2017), pp. 327-339.

[17] D. Rickard, S. Grimes, I. Butler, A. Oldroyd, and K. L. Davies, "Botanical constraints on pyrite formation," *Chemical Geology*, vol. 236, (2007), pp. 228-246.

[18] D. W. Shoesmith, P. Taylor, M. G. Bailey, and D. G. Owen, "The formation of ferrous monosulfide polymorphs during the corrosion of iron by aqueous hydrogen sulfide at 21ºC," *Journal of the Electrochemical Society*, vol. 127, (1980), pp. 1007-1015.

[19] D. W. Shoesmith, "Formation, Transformation and Dissolution of Phases Formed on Surfaces," Electrochemical Society Meeting, (Ottawa, 1984).

[20] N. G. Harmandas and P. G. Koutsoukos, "The formation of iron(II) sulfides in aqueous solutions," *Journal of Crystal Growth*, vol. 167, (1996), pp. 719-724.

[21] W. Sun and S. Nešić, "Kinetics of corrosion layer formation: part 1—iron carbonate layers in carbon dioxide corrosion," *Corrosion*, vol. 64, (2008), pp. 334-346.

[22] G. Sauerbrey, "Verwendung von Schwingquarzen zur Wägung dünner Schichten und zur Mikrowägung," *Zeitschrift für physik*, vol. 155, (1959), pp. 206-222.

[23] C. Gabrielli, S. Joiret, M. Keddam, H. Perrot, N. Portail, P. Rousseau, *et al.*, "A SECM assisted EQCM study of iron pitting," *Electrochimica Acta*, vol. 52, (2007), pp. 7706-7714.

[24] R. Oltra and I. O. Efimov, "Calibration of an electrochemical quartz crystal microbalance during localized corrosion," *Journal of The Electrochemical Society*, vol. 141, (1994), pp. 1838-1842.

[25] R. Baboian, *Corrosion Tests and Standards: Application and Interpretation*, Second ed.（West Conshohocken, PA: ASTM International, 2005), p. 141.

[26] J. W. Mullin, *Crystallization*, 4th ed.（Oxford, U.K.: Butterworth-Heinemann, 2001).

[27] X. Y. Liu, "Generic Mechanism of Heterogeneous Nucleation and Molecular Interfacial Effects," in *Advances in Crystal Growth Research*, Amsterdam: Elsevier Science B.V., pp. 42-61, 2001.

[28] S. Nešić and K.-L. J. Lee, "A Mechanistic Model for Carbon Dioxide Corrosion of Mild Steel in the Presence of Protective Iron Carbonate Films—Part 3: Film Growth Model," *Corrosion*, vol. 59, (2003), pp. 616-628.

[29] Z. Ma, Y. Yang, B. Brown, S. Nešic, and M. Singer, "Investigation of precipitation kinetics of $FeCO_3$ by EQCM," *Corrosion Science,* vol. 141, (2018), pp. 195-202.

[30] W. Sun, S. Nešić, D. Young, and R. C. Woollam, "Equilibrium expressions related to the solubility of the sour corrosion product mackinawite," *Industrial & Engineering Chemistry Research,* vol. 47, (2008), pp. 1738-1742.

[31] O. M. Suleimenov and R. E. Krupp, "Solubility of hydrogen sulfide in pure water and in NaCl solutions, from 20 to 320°C and at saturation pressures," *Geochimica et Cosmochimica Acta*, vol. 58, (1994), pp. 2433-2444.

[32] Y. K. Kharaka, W. D. Gunter, P. K. Aggarwal, E. H. Perkins, and J. D. DeBraal, "SOLMINEQ.88: a computer program for geochemical modeling of water-rock interactions,"（Alberta Research Council, Edmonton, Alberta, Canada, Report 88-4227, 1988).